Damage Characterization in Rock Material Using AE

Patrick GANNE, André VERVOORT, Department of Civil Engineering, Katholieke Universiteit Leuven, Heverlee-Leuven, Belgium.
Martine WEVERS, Department of Metallurgy and Materials Engineering, Katholieke Universiteit Leuven, Heverlee-Leuven, Belgium.

Abstract. The evolution of the cumulative energy of AE (acoustic emissions) as function of the applied load during specific laboratory loading tests leads to a subdivision of the loading in different stages. The stages during the loading can be correlated with load thresholds. Two separate cases are studied: in the first case macro-compressive stresses and in the second case macro-tensile stresses induce damage. In each case, the respective stages of the loading and load thresholds are correlated with the damage levels. These damage levels are described using thin slices of samples which are merely loaded till specific stages of the loading. Based on these observations, damage evolution models both in the case of macro-compressive stresses and macro-tensile stresses are proposed and discussed.

1. Introduction

The brittle fracturing of rock is a progressive process which involves the initiation, growth, interaction and coalescence of (micro-) cracks leading to the formation of the macro-fracture. This fracturing process is still widely investigated to fully describe and better understand this fracture process [6, 9, 15]. The aim of these studies is to obtain an idea of which mechanisms occur internally in the rock material, when it is subjected to certain stress-levels. Hereby multiple tools such as microtomography [14], radiography [11], scanning electron microscopy [13], resistivity measurements [10] etc. are used.

Different stress thresholds, based on stress-strain curves during uniaxial compressive tests are defined in [3, 4]. Suggestions towards the physical interpretations such as the start of crack nucleation and the crack damage stress (i.e. start of the occurrence of unstable crack growth) are given for these stress thresholds. A corresponding mathematically formulation of the crack initiation and crack damage thresholds as function of the uniaxial compressive strength during uniaxial and triaxial tests is known [1]:

$$\sigma_1 - \sigma_3 = A\sigma_{ucs} \qquad (1)$$

where σ_1, σ_3, σ_{ucs} are respectively the major and minor principal stress at the threshold and the uniaxial compressive strength (UCS). In the case of crack initiation, A varies between 0.4 and 0.5. In the case of crack damage, A varies between 0.8 and 0.9.

A successful correlation between the stress thresholds (defined as in [3, 4]) with AE (acoustic emission) measurements is made [2] using a discrete element code (PFC). Furthermore, it is concluded [2] that the stress threshold of crack initiation and the stress threshold of crack interaction and coalescence are more accurately detectable based on the cumulative number of AE events than based on the stress-strain curves.

Other researchers preferred the study of thin slices as a tool to better understand and describe different fracture stages [12]. A few studies [6, 15] report an increasing crack

density when the differential stress exceeds respectively 50% and 60% of the UCS. In this stage, the increasing crack density is caused by crack nucleation as well as crack propagation. In a next stage, acceleration in the crack growth is reported.

This paper describes and discusses the evolution of the received cumulative AE energy in the case of sample failure due to macro-compressive stresses and macro-tensile stresses. In both cases, several load thresholds are defined on the basis of laboratory experiments. Furthermore, the micro-damage, corresponding to the load thresholds, is described by a systematic observation of thin slices in the case of macro-compressive stresses as well as in the case of macro-tensile stresses. In order to create macro-compressive stresses and macro-tensile stresses, a specific sample geometry is used, as described in the following paragraph.

2. Methodology

The rock material used in the tests is Belgian crinoidal limestone. This material is mainly composed of calcite, in various forms. Besides crinoids, the limestone contains also some other bioclasts. Another major constituent of the crinoidal limestone is micrite. This very fine-grained microcrystalline calcite makes up the matrix of the limestone [12, 13].

The crinoidal limestone blocks are sawed and rectified into rectangular slabs of 31 mm x 60 mm x 140 mm. At one side, half a cylinder is drilled with a diameter of 58 mm (Figure 1). The loading direction determines the stress redistribution. If the external load is applied on the short sides of the rectangular samples, compressive stresses are present adjacent to the borehole. Figure 2A shows the calculations (Flac 4.0) of the stress redistribution on the symmetrical plane when a loading force of 80 kN (about 80% of the failure load) is applied on the short sides of a sample. This is further called the compression configuration. If the external load is applied on the long sides, both the radial and tangential stress are negative (tensile stresses) next to the borehole. Figure 2B shows the calculations of the stress redistribution on the symmetrical plane when the load on the long sides of a sample rises until plastic deformation occurs (at an external load of 40 kN). It has been checked that the zone of tensile stresses extends at the borehole from position -45° till +45° ('position angle' is defined in Figure 4). This is further called the tension configuration.

The Dartec loading machine is used in the displacement-controlled mode (v = 0.001 mm/s). During the loading test, a 1 mm thick Teflon sheet is placed between the machine compression platens and the test samples, in order to minimize the frictional stresses. Acoustic emissions (AE) are continuously recorded during each loading using the AMS3 system of Vallen System GmbH. Two wide-band AE sensors of type B1025 (Digital Wave Corp.) having a frequency range from 50 kHz to 2 MHz are attached to the test samples, as shown in Figure 1. The distance between the AE sensors in the compression configuration and in the tension configuration is about 60 and 40 mm respectively. The preamplifier is set on 49 dB and a threshold of 16 dB is used ($dB = 20\log(\frac{Voltage[\mu V]}{1\mu V})$). The set-up of the sensors allows a linear localisation of AE sources. The velocity of the longitudinal elastic wave used for the location calculations is taken as 5700 m/s [5, 7]. Only AE events occurring in the central zone (30 mm in the tension configuration and 50 mm in the compression configuration) and with a received peak amplitude higher than 22 dB are considered.

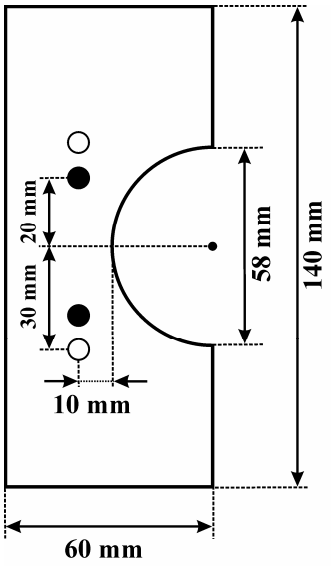

Figure 1. Geometry of the tested samples, the thickness of the samples is 31 mm. The position of the attached AE sensors is indicated in the case of compression configuration (O) and in the case of tension configuration (●).

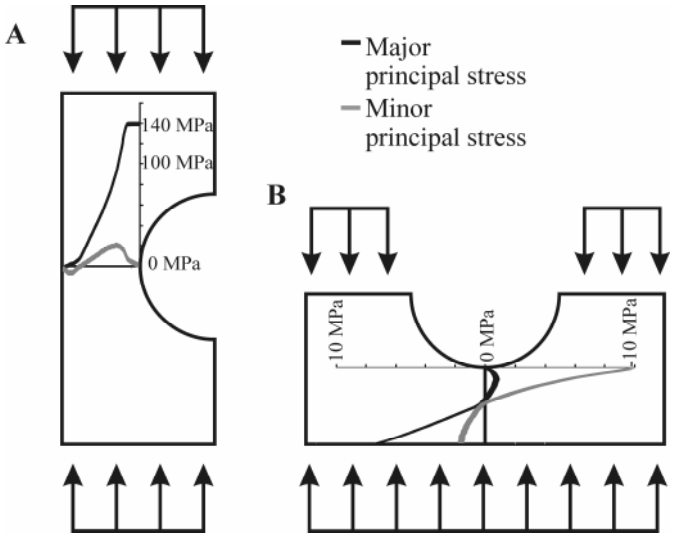

Figure 2. Presence of tensile stresses (negative) and compressive stresses (positive) in the test samples, depending on the load direction: (A) in compression configuration and (B) in tension configuration.

Prior to preparing thin slices, the samples are impregnated under vacuum with a fluorescent resin. Thin slices with a thickness of 30 µm are prepared. Figure 3 shows the position of the thin slice in each sample. The thin slice is taken in the middle of the thickness. This is the most likely damaged region. A zone of 20 mm tangentially and 6 mm wide (radial direction) is digitally photographed with a pixel resolution of 0.5 µm. By composing semi-automatically one mosaic photograph, the pixel accuracy decreases to 1%. The cracks are semi-automatically recorded in the final photograph. As the cracks are not always easy to observe on the digital photographs, manual decisions are taken after looking through the transmitted light and the reflection fluorescence microscope (x5). For each visible crack, the position of the central and the end points (defined by the radial distance and the angle of the position), the orientation (i.e. the absolute value of the angle between the orientation of the crack and the radial direction) and the length are recorded (Figure 4). As the direction of intergranular cracks frequently changes, the intergranular cracks are subdivided into multiple smaller (length > 15 µm) straight cracks. Because of the symmetry in the sample configuration, in the external loading and in the stress redistribution, only the absolute value of the orientation is considered. The definitions, as well as the calculation methodologies are in correspondence to [8]. An interesting feature in the statistical analyses is for example the total length of cracks within a specific orientation range: the length of all cracks which orientation is within this specific range is summed. This information is summarised in a graph of total length of all cracks within crack orientation ranges as a function of these orientation ranges and is referred to as ‘cumulative length as a function of the crack orientation’.

In all samples, numerous cracks occur within a 0.5 mm band around the borehole. In this band, the dominant orientation of the cracks is 80° ± 10° (i.e. tangential orientation). These cracks, within this band of 0.5 mm, are interpreted as a result of the drilling of the borehole (Figure 3). So, these cracks are not considered in the further analyses [5].

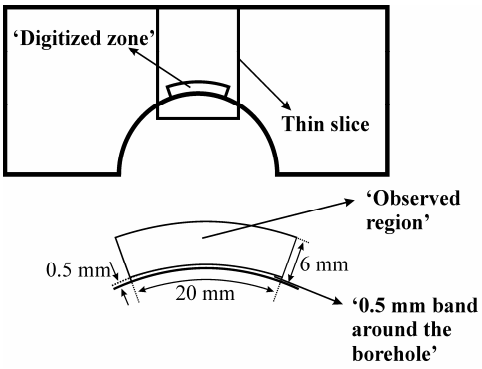

Figure 3. Location of the thin slice, in the middle of the thickness. The digitized zone, the observed region and the 0.5 mm band around the borehole are defined.

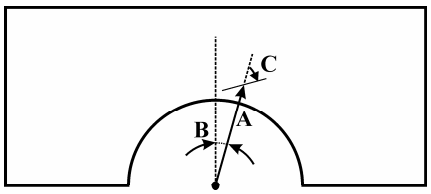

Figure 4. Parameters describing a crack (radial distance A, position angle B and orientation C (i.e. the direction relative to the radial direction)).

3. Results and Interpretations

3.1 Evolution of Damage in Compression Configuration

3.1.1 Evolution of the Recorded AE Cumulative Energy

Two test samples (C^{ci}_a and C^{ci}_b) are loaded in the compression configuration until failure. Based on the evolution of the recorded cumulative AE energy, four stages during the loading in compression configuration can be distinguished (Figure 5):

(1) No AE are registered.
(2) After the first registered AE, the cumulative AE energy rises linearly as function of the applied load.
(3) A first increase of the slope of the cumulative AE energy as function of the applied load can be noticed. This stage is called the systematic crack formation and growth.
(4) A second increase of the slope of the cumulative AE energy as function of the applied load can be noticed. This stage is called the crack interaction and coalescence.

The transitions between two successive stages are referred to as load thresholds:

(1) The force at the first registered AE (fae).
(2) The force when the systematic crack formation and growth (sc) starts.
(3) The force when the crack interaction and coalescence (ci) starts.

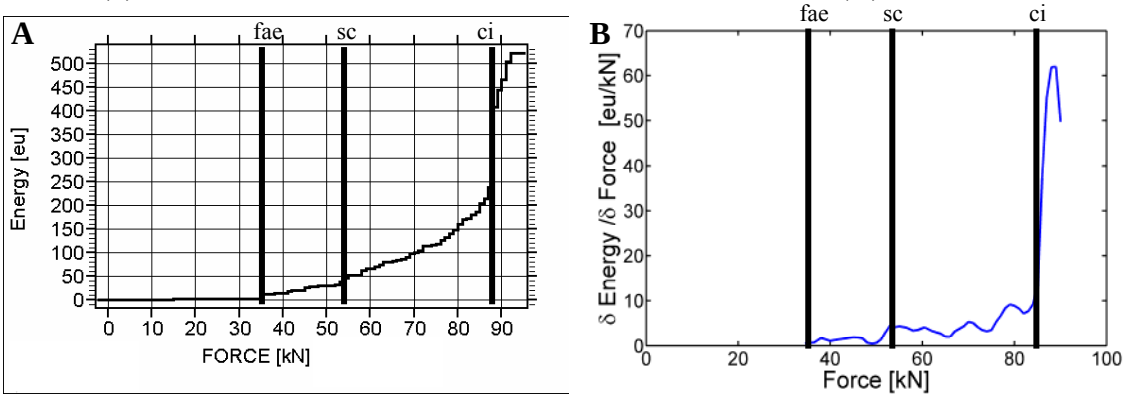

Figure 5. (A) Graph of the recorded cumulative energy [eu] as function of the external applied force [kN] during the loading of C^{ci}_a (until failure). (B) Graph of the derivative of the recorded cumulative energy by the external applied force [eu/kN] as function of the external applied force [kN] during the loading of C^{ci}_a (until failure). The bars indicate the load thresholds (fae, sc and ci; see text for explanation).

The nomenclature of the stages and of the load thresholds is in correspondence with [2], where a PFC model of uniaxial and triaxial loadings is discussed. This results in the definition of stress thresholds (first AE, systematic crack formation and growth, crack interaction and coalescence), based on a 'stepwise linear' interpolation of the graph of the cumulative number of AE events (logarithmic) versus applied stress (logarithmic). Figure 5A and B shows that in this study, the load thresholds are defined using a 'stepwise linear' interpolation in the graph of the (linear) cumulative energy of AE versus (linear) applied force.

Table 1 summarises the maximal applied force and the total registered cumulative energy [eu] of the samples C^{ci}_a, C^{ci}_b, C^{sc}, C^{fae} (loaded in compression configuration) and U. The detected load thresholds [kN] (fae, sc and ci) are calculated in Table 2. The loading of C^{sc} and C^{fae} is stopped at 83 kN and 44 kN respectively (no macro-failure is observed). Remark that C^{sc} is loaded beyond the load threshold of the start of the systematic crack formation and growth. Furthermore, C^{fae} is loaded beyond the load threshold of first AE. U is a reference sample, which is not loaded. U is used to differentiate the induced crack by loading and artefacts like natural cracks and cracks induced by the sawing, rectifying, drilling, thin slice preparation, etc.

Table 1. Overview of the maximal applied force and the total registered cumulative energy [eu] (Σ energy) of the different samples loaded in the compression configuration.

Sample	maximal applied load	Σ energy
C^{ci}_a	95 kN (100%)	530 eu
C^{ci}_b	105 kN (100%)	730 eu
C^{sc}	83 kN (83%$^{\#}$)	150 eu
C^{fae}	44 kN (44%$^{\#}$)	100 eu
U	0 kN (0%)	0 eu

$^{\#}$ in these cases, the failure load is not experimentally obtained. A failure load equal to the mean of the failure load of C^{ci}_a and C^{ci}_b (i.e. 100 kN) is assumed in the calculations.

Table 2. Overview of the load threshold [kN] of the first AE (fae), of the start of the systematic crack formation and growth (sc), of the start of the crack interaction and coalescence (ci) and the maximal applied force (maf) of the different samples loaded in the compression configuration. The forces compared to the force at failure are indicated in percent in brackets.

Sample	fae	sc ± 4kN	ci ± 4kN	maximal applied load
C^{ci}_a	35 kN (37%)	53 kN (56%)	86 kN (90%)	95 kN (100%)
C^{ci}_b	35 kN (37%)	61 kN (58%)	90 kN (86%)	105 kN (100%)
C^{sc}	28 kN (28%$^{\#}$)	62 kN (62%$^{\#}$)	--*	83 kN (83%$^{\#}$)
C^{fae}	23 kN (23%$^{\#}$)	--*	--*	44 kN (44%$^{\#}$)
U	--*	--*	--*	0 kN (0%)

$^{\#}$ in these cases, the failure load is not experimentally obtained. A failure load equal to the mean of the failure load of C^{ci}_a and C^{ci}_b (i.e. 100 kN) is assumed in the calculations.
*-- indicates that the loading do not exceed the specific load threshold.

Table 2 shows that the load threshold of the first registered AE is between 23% and 37% of the failure load. The large spreading is caused by the fact that the load where the first AE is registered is function of e.g. the coupling of the sensors. The load threshold of the start of the systematic crack formation and growth varies between 56% and 62% of the failure load. The load threshold of the start of the crack interaction and coalescence varies between 86% and 90% of the failure load. Other measurements confirm these percentages and the described evolution of the cumulative AE energy.

3.1.2 Study of the Thin Slices

Samples C^{ci}_a and C^{ci}_b are loaded till macro-failure. The normally digitized region around the borehole is pulverised to a large extend. So, it is not useful to prepare a thin slice of these samples. Thin slices of C^{sc}, C^{fae} and U are prepared and studied. In these samples,

including the U-sample, numerous intragranular cracks are observed but no intergranular crack is observed.

Table 3 gives an overview of some statistical properties of the crack in the observed regions. The damage level of C^{fae} is not higher than the damage level of U. Only the mean crack length slightly increases (51.0 µm (U) versus 67.2 µm (C^{fae})). The actual decrease of the cumulative length of cracks in C^{fae} (30 mm (C^{fae}) versus 42 mm (U)) is interpreted as resulting from the heterogeneity in natural rock samples. Though, sample C^{fae} is loaded till about 44% of the failure load and a total cumulative energy of 100 eu is recorded (i.e. 16% of the cumulative energy recorded on C^{ci}_a or C^{ci}_b). Figure 6 compares the cumulative length as a function of the crack orientation in the observed regions of U, C^{fae} and C^{sc}. In samples U and C^{fae}, the cracks are not preferentially oriented. These observations confirm that as the applied load does not exceed the load threshold of systematic crack formation and growth, no significant amount of cracks occur or grow.

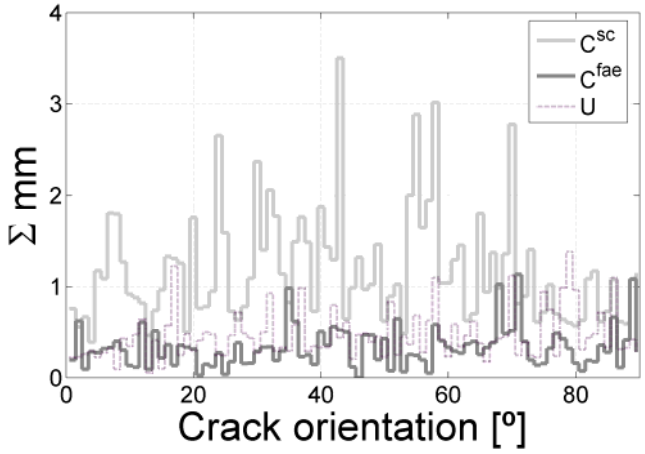

Figure 6. Comparison of the cumulative length as a function of the crack orientation in the observed regions of U, C^{fae} and C^{sc} .

Table 3 shows that more damage in C^{sc} than in C^{fae} and U is observed: more and longer cracks results in a higher cumulative length of (intragranular) cracks (108 mm (C^{sc}) versus 42 mm (U) and 30 mm (C^{fae})). Most of the cracks are activated cleavage planes of crystals, which diameter can amount till 1 mm. Several crystals have systematic parallel and cross slipping activated cleavage planes. Apart from these crystals, the cracks are scattered over the entire observed region. These facts suggest that if the applied load does exceed the load threshold of systematic crack formation and growth, numerous intragranular cracks occur and grow. Figure 6 shows that the cracks in the observed region in C^{sc} are preferentially oriented (in contrast to U and C^{fae}) in a broad range from 25° to 70°. Considering the principal stress orientation in the vicinity of the borehole, the general theory of Mohr-Coulomb predicts the occurrence of a macro-fracture with an orientation of about 60°.

Table 3. Comparison between statistical properties of the cracks in the observed regions of U, C^{fae} and C^{sc}.

	U	C^{fae}	C^{sc}
Σ length of cracks [mm]	42 (100%)	30 (100%)	108 (100%)
INTERGRANULAR CRACKS Σ length of intergranular cracks [mm]	0 (0%)	0 (0%)	0 (0%)
INTRAGRANULAR CRACKS Σ length of intragranular cracks [mm]	42 (100%)	30 (100%)	108 (100%)
Number of intragranular cracks	831	439	1319
Arithmetic mean of the length [µm] of intragranular cracks	51.0	67.2	82.1
Σ length of intragranular cracks > 0.1 mm [mm]	12	11	55

3.2 Evolution of Damage in Tension Configuration

3.2.1 Evolution of the Recorded AE Cumulative Energy

T^{ca} is loaded in the tension configuration until a macro-failure (i.e. an intergranular crack) occurs. Three stages can be distinguished, based on the evolution of the recorded cumulative AE energy during the loading in tension configuration (Figure 7):

(1) No AE is registered.

(2) After the first registered AE, the cumulative AE energy increases as a convex function of the applied load.

(3) The final stage is characterised by a concave evolution of the cumulative AE energy as a function of the applied load.

The transitions between two successive stages are referred to as load thresholds:

(1) The force at the start of the convex evolution (ce).

(2) The force at the start of the concave evolution (ca).

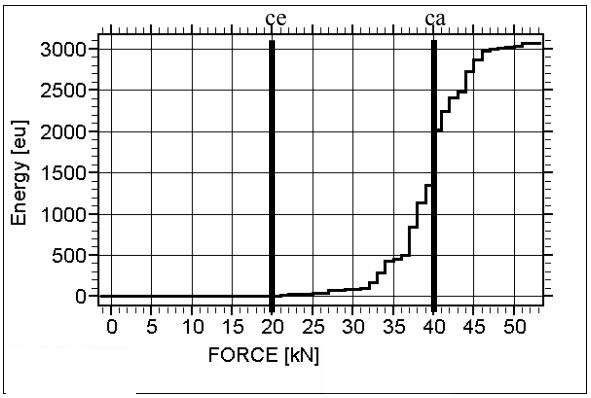

Figure 7. Graph of the recorded cumulative energy [eu] as function of external applied force [kN] during the loading of T^{ca} (until macro-fracture). The bars indicate the load thresholds (ce and ca; see text for explanation).

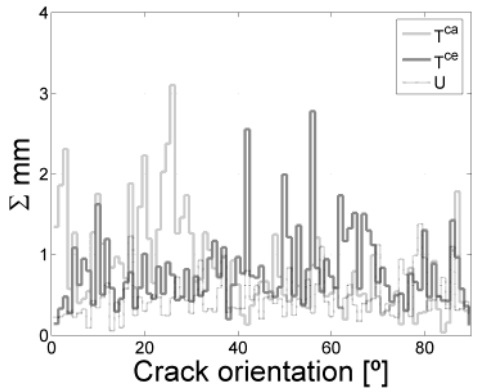

Figure 8. Graph of the cumulative length as a function of the crack orientation in the observed regions of U, T^{ce} and T^{ca}.

T^{ce} is a sample, damaged in the tension configuration, where the loading is stopped at 12 kN (no macro-fracture is observed), see Table 4. T^{ce} is loaded beyond the load threshold of the start of the convex evolution. Remark that in sample T^{ca} the start of the convex evolution is at about 50% of the start of the concave evolution. Other samples confirm that the load at the start of the convex evolution is at 60% ± 10% of the load at the start of the concave evolution of the cumulative AE energy.

Table 4. Overview of the maximal applied force and the total registered cumulative energy [eu] (Σ Energy) of the different samples loaded in the tension configuration.

Sample	maximal applied force	Σ Energy
T^{ca}	52 kN	3100 eu
T^{ce}	12 kN	80 eu
U	0 kN	0 eu

Table 5. Overview of the threshold force [kN] of the start of the convex evolution (ce), the start of the concave evolution (ca), the maximal applied force (maf) and the total registered cumulative energy [eu] (Σ Energy) of the different samples loaded in the tension configuration.

Sample	ce ± 4kN	ca ± 4 kN	maximal applied force
T^{ca}	20 kN	40 kN	52 kN
T^{ce}	5 kN	--*	12 kN
U	--*	--*	0 kN

*-- indicates that the loading does not exceed the specific load threshold.

3.2.2 Study of the Thin Slices

In this section, thin slices of T^{ca}, T^{ce} and U are studied. In T^{ce} and U, only intragranular cracks are observed. In contrast, in T^{ca} both intragranular and intergranular cracks are observed.

Although in T^{ce} only 3% of the cumulative AE energy (in comparison to T^{ca}) is recorded, T^{ce} is more damaged than U (Table 6). Approximately the same number of cracks is observed, but the mean length of the cracks has increased (51.0 µm (U) versus 87.7 µm (T^{ce})). Most of the observed intergranular cracks are activated cleavage planes. The cumulative length as a function of the crack orientation in the observed region of T^{ce} increases between 0° and 70° (Figure 8). These observations suggest that the early AE are generated by the growth of activated cleavage planes which have an orientation of between 0° and 70°. Considering the principal stress orientation in the vicinity of the borehole, a radial (i.e. 0°) tensile macro-fracture seems logic.

Table 6. Comparison between statistical properties of the cracks in the observed regions of U, Tce and Tca.

	U	**T^{ce}**	**T^{ca}**
Σ length of cracks [mm]	42 (100%)	73 (100%)	73 (100%)
INTERGRANULAR CRACKS			
Σ length of intergranular cracks [mm]	0 (0%)	0 (0%)	21 (29%)
INTRAGRANULAR CRACKS			
Σ length of intragranular cracks [mm]	42 (100%)	73 (100%)	52 (100%)
Number of intragranular cracks	831	828	679
Arithmetic mean of the length [µm] of intragranular cracks	51.0	87.7	76.1
Σ length of intragranular cracks > 0.1 mm [mm]	12	38	23

The damage in T^{ca} is characterised by a 21 mm long intergranular crack. The intergranular crack is approximately radially oriented (0°) and reaches the borehole 3 mm off centre. The intergranular crack goes along grain boundaries as well as along cleavage planes of crystals. The grains around the intergranular crack (till somewhat 0.5 mm) are damaged by intragranular cracks. Further from the intergranular crack, the amount of intragranular cracks barely exceeds the amount of damage in the reference sample U. Table 6 shows that the cumulative length of intragranular cracks (52 mm (T^{ca})) has decreased in comparison with T^{ce} (73 mm). It is possible that numerous intragranular cracks have grown and that they form the intergranular crack. So, these cracks are not counted as intragranular cracks anymore. Figure 8 shows an increase of the cumulative length of cracks which have an orientation of less than 10° and from 20° till 30°. These observations suggest that if the applied load exceeds the start of the concave evolution, the interaction of the intragranular cracks leads to the formation of the intergranular crack, which is preferentially radially (i.e. 0°) oriented.

4. Conclusions

Using the evolution of the cumulative energy of recorded AE and a thorough study of thin slices, two damage models (one in the case of macro-compressive stresses and one in the case of macro-tensile stresses) are proposed.

In the case of macro-compressive stresses, four stages during the loading can be distinguished based on the cumulative AE energy evolution: (1) no AE is registered, (2) the stage of the first AE, (3) the stage of the systematic crack formation and growth, (4) the stage of the crack interaction and coalescence. The transition of these stages defines three load thresholds: (1) the force at the first registered AE (at 23% till 37% of the failure load),

(2) the force when the systematic crack formation and growth start (at 56% till 62% of the failure load) and (3) the force when the crack interaction and coalescence start (at 86% till 90% of the failure load). When the applied load does not exceed the threshold of the start of the systematic crack formation and growth, no significant amount of cracks occurs or grows. Once the applied load exceeds the threshold of the start of the systematic crack formation and growth, a lot of intragranular cracks occur and grow. These cracks are preferentially oriented in a broad range from 25° to 70°. When the applied load exceeds the threshold of the start of the crack interaction and coalescence, unstable crack formation causes the macro-failure of the sample.

In the case of macro-tensile stresses, three stages are recognised: (1) no AE is registered, (2) a convex evolution of the cumulative AE energy as function of the applied load, (3) a concave evolution of the cumulative AE energy as function of the applied load. The transition of these stages defines two load thresholds: (1) the force of the start of the convex evolution and (2) the force of the start of the concave evolution. The force of the start of the convex evolution is at about 50% of the start of the concave evolution. The early AE are generated by the growth of activated cleavage planes which are already partially activated. Around the load threshold of the start of the concave evolution, an intergranular crack grows in an unstable way in the radial direction.

Acknowledgements

The financial support of the Research Council of the Katholieke Universiteit Leuven (OT-project) is gratefully appreciated.

References

[1] Cai M., Kaiser P.K., Tasaka Y., Maejima T., Morioka H. and Minami M., 2004. Generalized crack initiation and crack damage stress thresholds of brittle rock masses near underground excavations. Int. J. Rock Mech. Min. Sci. 41, 833-847.
[2] Diederichs M.S., Kaiser P.K. and Eberhardt E., 2004. Damage initiation and propagation in hard rock during tunnelling and the influence of near-face stress rotation. Int. J. Rock Mech Min Sci. 41, 785-812.
[3] Eberhardt E., Stead D. and Stimpson B., 1999. Quantifying progressive pre-peak brittle fracture damage in rock during uniaxial compression. Int. J. Rock Mech. Min. Sci. 36, 361-380.
[4] Eberhardt E., Stimpson B. and Stead D., 1999. Effects of grain size on the initiation and propagation thresholds of stress-induced brittle fractures. Rock Mech. Rock Engng., 32, 81-99.
[5] Ganne P. and Vervoort A., 2006. Characterisation of tensile damage in rock samples induced by different stress paths. Pure and Appl. Geophys., 163, in press.
[6] Homand F., Hoxha D., Belem T., Pons M.N. and Hoteit N., 2000. Geometric analysis of damaged microcracking in granites. Int. J. Rock Mech. Min. Sci. 32, 361-376.
[7] Lavrov A, Vervoort A., Wevers M. and Napier J.A.L., 2002. Experimental and numerical study of the Kaiser effect in cyclic Brazilian tests with disk rotation. Int. J. Rock Mech. Min. Sci. 39, 287-302.
[8] Russ J.C., 2002. The Image Processing Handbook. Fourth Edition. CRC Press, London, 771p.
[9] Sangha C.M., Talbot C.J. and Dhir R.K., 1974. Microfracturing of a sandstone in uniaxial compression. Int. J. Rock Mech. Min. Sci. & Geomech. Abstr. 11, 107-113.
[10] Van de Steen B., Wuytens B., Vervoort A. and Van Gemert D., 1998. Evaluation of mineral building materials: problems related to resistivity methods. RILEM, Material and Structures 31, 126-132.
[11] Van de Steen B. and Wevers M., 1998. Acoustic emission preceding macrocrack formation in samples containing a stress concentrator. Proceeding of the third international conference on mechanics of jointed and faulted rock. Rossmanith H.P., editor, 387-392.
[12] Van de Steen B., 2001. Effect of heterogeneity and defects on the fracture pattern in brittle rock. PhD thesis, KULeuven, Leuven, 249p.
[13] Van de Steen B., Vervoort A. and Sahin K., 2002. Influence of internal structure of crinoidal limestone on fracture paths. Eng. Geol. 67, 109-125.
[14] Vervoort A., Wevers M., Swennen R., Roels S., Van Geet M. and Sellers E., 2004. Recent advances of X-ray CT and its applications for rock material. In: X-ray CT for Geomaterials, Swets & Zeitlinger, Lisse, 79-91.
[15] Zhao Y., 1998. Crack pattern evolution and a fractal damage constitutive model for rock. Int. J. Rock Mech. Min. Sci. 35, 349-366.